Noninvasive Imaging for Monitoring of Viable Cancer Cells Using a Dual-Imaging Reporter Gene

Jae Hoon Shin, MS[1–3]; June-Key Chung, MD, PhD[1–3]; Joo Hyun Kang, PhD[1,3]; Yong Jin Lee, MS[1–3]; Kwang Il Kim, MS[1–3]; Young So, MD, PhD[1]; Jae Min Jeong, PhD[1,3]; Dong Soo Lee, MD, PhD[1,3]; and Myung Chul Lee, MD, PhD[1]

[1]Department of Nuclear Medicine, Seoul National University Hospital, Seoul, Korea; [2]Department of Tumor Biology, Seoul National University College of Medicine, Seoul, Korea; and [3]Laboratory of Molecular Imaging and Therapy of Cancer Research Institute, Seoul National University College of Medicine, Seoul, Korea

Molecular imaging methods have been used recently to investigate biologic events. To develop a molecular imaging method suitable for monitoring viable cancer cells, we made a dual-imaging reporter gene system and examined the correlation between cancer cell number and signals from 2 reporter genes, sodium iodide symporter (NIS) and luciferase. **Methods:** NIS and luciferase genes were linked with the internal ribosomal entry site and transfected into SK-HEP1 cells to generate SK-HEP1-NL cells. ^{125}I uptake assays, luciferase assays, and scintigraphic and luminescence imaging were performed on SK-HEP1-NL cells. After treating with doxorubicin, cell counting, assays, and imaging were performed. SK-HEP1 and SK-HEP1-NL cells were inoculated subcutaneously into the flanks of nude mice. After incubation, scintigraphic and luminescence images were acquired and quantitated. **Results:** The results of radioiodide uptake, luciferase assay, and scintigraphic and luminescence imaging in vitro correlated well with viable cell numbers. Upon increasing the concentration of doxorubicin, cell numbers decreased, and this correlated with a decrease in radioactivity and luminescence intensity. The radioactivity from in vivo scintigraphic images and the intensity from luminescence images were also found to be proportional to the tumor weight. **Conclusion:** The developed dual-reporter imaging method using NIS and the luciferase gene reflected viable cancer cell numbers and could detect changes in cell number after doxorubicin treatment.

Key Words: reporter gene; sodium iodide symporter; luciferase; molecular imaging; drug development

J Nucl Med 2004; 45:2109–2115

It is important to be able to determine viable cancer cell numbers and to monitor changes after therapeutic intervention in the fields of cancer research and clinical oncology. Though many investigations have been performed on cancer biology and on anticancer drug development, few methods are available for monitoring the therapeutic effect (e.g., 3-(4,5-dimethyl-2-thiazolyl)-2,5-diphenyltetrazolium bromide (MTT) assay for metabolism, thymidine uptake assay for proliferation (*1*), and trypan-exclusion cell count for viable cell count). Moreover, these conventional assay tools can provide useful information only at the in vitro level.

Imaging methods based on optical systems, such as bioluminescence and fluorescence, can play a role in detecting viable cancer cells and in evaluating the kinetics of tumor-cell clearance after anticancer therapy in vitro and in vivo (*2–5*). The advantages of this approach are (a) the simplicity of quantifying the viable cell count, (b) the possibility of acquiring noninvasive and real-time data, (c) the possibility of making multiple determinations during the disease course in a single animal, (d) the possibility of optimizing therapy (choice of modality, combination therapy, route of administration) because external signals are proportional to the tumor-cell burden, and (e) the ability to detect small cell numbers (>2,500 tumor cells). Despite of these advantages, optical imaging methodologies are limited in terms of clinical application because their tissue-penetrating abilities are poor.

The sodium iodide symporter (NIS) is one nuclear imaging reporter gene that could be used to overcome the limitations of optical imaging strategies. NIS is a transmembrane protein, which actively transports iodide ions into thyroid cells (*6*). The accumulation of radioiodine in specific cells or tissues mediated by the NIS gene transfer shows its possibilities for molecular imaging (*7–12*). An imaging system based on the NIS gene can produce images with commonly used radionuclides, such as ^{123}I, ^{125}I, or ^{99m}Tc-pertechnetate, and simple γ-camera systems.

The present study was undertaken to develop a noninvasive method for monitoring viable cancer cell numbers using the dual-reporter gene and to investigate the correlation between cell number and reporter gene expression both

Received Mar. 19, 2004; revision accepted Jul. 30, 2004.

For correspondence or reprints contact: June-Key Chung, MD, PhD, Department of Nuclear Medicine, Seoul National University Hospital, 28, Yongon-dong, Chongno-gu, Seoul 110-744, Korea.

E-mail: jkchung@plaza.snu.ac.kr

in vitro and in vivo. We constructed a reporter vector that linked the NIS and luciferase using the internal ribosomal entry site (IRES). After producing a stable cell line by transferring the reporter vector, the signals of both reporters were evaluated using radionuclide-based and optically based methods in vitro and in vivo.

MATERIALS AND METHODS

Recombinant DNA Plasmid Construct

pIRES-NL, containing human NIS (hNIS) and luciferase, was made by inserting hNIS and luciferase into pIRES vector (Clontech). hNIS, cloned into pCDNA3 (Invitrogen), was kindly provided by Dr. Sissy Jhiang (Ohio State University). The coding sequence fragment of hNIS was cloned using the polymerase chain reaction with forward primer 5′-CGGCTCGAGATGGAGGCCGTGGAGACC-3′ and reverse primer 5′-GGCCACGCGTTCAGAGGTTTGTCTCCTGCT-3′. The fragment was inserted upstream of the IRES sequence in pIRES vector after digestion with *Xho* I and *Mlu* I (Intron). Luciferase was cloned from pGL2 vector (Promega) into downstream of the IRES sequence using the same method as that used for hNIS except for the use of forward primer 5′-CCGGGTCGACATGGAAGACGCCAAAAACAT-3′, reverse primer 5′-CCGGGCGGCCGCTTACAATTTGGACTTTCCGC-3′, restriction enzyme *Sal* I, and *Not* I (Intron).

Cell Culture and Stable Cell Line Generation

The human hepatocellular carcinoma cell line SK-HEP1 and transfectants were cultured in RPMI 1640 medium (WelGENE, Inc.) supplemented with 10% fetal bovine serum and 1% penicillin and streptomycin solution (GIBCO). After pIRES-NL had been transfected into SK-HEP1 cells using the liposome formulation Lipofectamine plus (Invitrogen), according to the manufacturer's instructions, SK-HEP1-NL cells expressing NIS and luciferase stably were generated at under 1,000 μg/mL G418 (Invitrogen) selection.

Radioactive Iodide Uptake Assay

Radioactive iodide uptake studies were performed at 37°C using a modification of the method described by Weiss et al. (*13*). A dilution series of SK-HEP1 and SK-HEP1-NL cells were inoculated into 24-well plates over a range of 3×10^4 to 5×10^5 cells per plate. After a 12-h incubation, the ^{125}I uptake level was examined. The iodide uptake level was determined by incubating the cells with 500 μL Hanks' balanced salt solution (HBSS) containing 0.5% bovine serum albumin, 10 mmol/L 2-(4-[2-hydroxyethyl]-1-piperazinyl)ethanesulfonic acid-NaOH, pH 7.4, and 3.7 kBq (0.1 μCi) Na^{125}I at 37°C for 20 min. After incubation, the cells were washed twice as quickly as possible (<15 s) with 2 mL of iodide-free ice-cold HBSS buffer. Cells were detached with 500 μL trypsin, and the radioactivity was measured using a γ-counter (Canberra Industries).

In Vitro γ-Camera Imaging

The uptake of ^{99m}Tc-pertechnetate, another radiotracer transported by NIS, was determined using the same procedure as that used for radioiodine uptake. After incubation with 370 kBq (10 μCi) ^{99m}Tc-pertechnetate, the cells were washed twice as quickly as possible with 2 mL of radiotracer-free ice-cold HBSS. Afterward, the 24-well plate was placed under a γ-camera (ON 410; Ohio Nuclear) equipped with a pinhole collimator and scanned for 5 min.

Luciferase Assay

For the in vitro luciferase assay, a dilution series of SK-HEP1 and SK-HEP1-NL cells were inoculated into 24-well plates over a range of 3×10^4 to 5×10^5 cells per plate. After a 12-h incubation, each well was washed with phosphate-buffered saline (PBS). The luciferase assay was performed using a Luciferase Assay Kit (Applied Biosystems). Lysis solution was added to each well, and cells were detached from the plate with a cell scraper. The cell lysate was then transferred to a microplate and bioluminescence was measured using a microplate luminometer (TR717; Applied Biosystems)

In Vitro Bioluminescent Imaging

For in vitro bioluminescent imaging, a dilution series of SK-HEP1 and SK-HEP1-NL cells were inoculated into 24-well plates over the range 3×10^4 to 5×10^5 cells per plate. After a 12-h incubation, each well was washed with PBS. Bioluminescent images were acquired using a Bright-Glo luciferase assay system (Promega) and LAS-3000 equipped with a cooled charge-coupled device (CCD) camera (Fuji Film). According to the manufacturer's instructions, 100 μL of a mixture of luciferin and buffer solution was added on each well. After incubation for 10 min, the plate was placed in the dark box and the gray-scale image was acquired. Bioluminescence was collected for 5 min. Rainbow-scale pseudocolor images were converted and superimposed over the gray-scale-shape image and processed using graphic software (Photoshop; Adobe). Quantification analysis of the acquired bioluminescent images was performed using an image analysis program, Multi Gauge vs 2.02 (Fuji Film). To prevent distortion of data, quantification analysis was performed under no modification of the raw image. The optical density (OD) of the region of interest (ROI) on the gray-scale image was measured by the image analysis program. The same size of ROI was selected for comparison, and the OD of the background was subtracted on each well plate.

In Vitro Assays After Doxorubicin Treatment

Doxorubicin was used to evaluate the therapeutic effect. SK-HEP1 and SK-HEP1-NL cells were inoculated into a 24-well plate (5×10^5 cells per well). After 12 h, the medium was replaced with fresh medium containing 0, 0.5, 1, 2, 5, and 10 μg/mL of doxorubicin and cells were incubated in 5% CO_2 for 24 h at 37°C. Viable cells were then counted using the trypan blue–exclusion method. The bioluminescent assay, bioluminescent image acquisition, radioiodide uptake assay, and nuclear image acquisition were performed according to the methods described with minor modifications. The correlation between cancer cell numbers and measured values was performed using Excel 2002 (Microsoft).

Animal Experiments

Animal experiments were performed with the approval of the Seoul National University Animal Research Committee. Male BALB/c nude mice, 3 wk old, were maintained at our facility under specific pathogen-free conditions. SK-HEP1 and SK-HEP1-NL cells were xenografted subcutaneously into the left fore flank (SK-HEP1; 5×10^6 cells), right fore flank (SK-HEP1-NL; 5×10^6 cells), left hind flank (SK-HEP1-NL; 1×10^7 cells), and right hind flank (SK-HEP1-NL; 5×10^6 cells) of each nude mouse. After allowing 2 wk for tumor growth, bioluminescent and γ-camera images were acquired. Anesthesia was performed by an intraperitoneal injection of 40 μL of ketamine and xylazine (4:1) solution. Luciferin was prepared by dissolving the luciferin potas-

sium salt (Molecular Probes). An aqueous solution of luciferin was injected into the peritoneal cavity 10 min before imaging, and the animal was placed in the dark box of LAS-3000 film (Fuji Film). After gray-scale images under white light had been acquired, bioluminescent images were acquired by collecting and integrating the light for 10–15 min. Image processing and analysis were performed as described previously, and the γ-camera images were acquired. Thirty minutes after injecting 11.1 MBq (300 μCi) of ^{99m}Tc-pertechnetate into the tail vein, mice with tumors were placed in a spread-prone position and scanned with a γ-camera (ON 410; Ohio Nuclear) equipped with a pinhole collimator.

RESULTS

Correlation Between Radioactivity and Cell Number

The SK-HEP1-NL cell line, which stably expresses NIS and luciferase, was generated for this study. Figure 1 shows the result of radioiodide uptake and γ-camera images in a dilution series of SK-HEP1-NL and SK-HEP1 cells. As the numbers of SK-HEP1-NL were increased, radioiodide uptakes were also increased (Fig. 1A). A high correlation (r^2 = 0.9987) was observed between radioiodide uptake and cell number (Fig. 1B). Increased radioactivity was also observed in γ-camera images. According to increases in the numbers of SK-HEP1-NL cells, the accumulation of ^{99m}Tc-pertechnetate also increased (Fig. 1C). An analysis of intensities in the ROI indicated a high correlation (r^2 = 0.9775) between intensity and cell number (Fig. 1D).

Correlation Between Bioluminescence and Cell Number

Figure 2 shows the result of bioluminescence and bioluminescent images produced using a luminometer and a highly sensitive cooled CCD camera, respectively. As the numbers of SK-HEP1-NL cells were increased, the bioluminescence increased (r^2 = 0.9979); SK-HEP1 showed a very low level of luminescence in cells (Figs. 2A and 2B). The increase of bioluminescence on increasing cell number was also demonstrated by bioluminescence imaging (Fig. 2C). The analysis of intensities in the ROI indicated a high correlation (r^2 = 0.9984) between intensity and cell number (Fig. 2D).

Monitoring of Therapeutic Intervention In Vitro

Treatment with doxorubicin killed both SK-HEP1 and SK-HEP1-NL cells in vitro and reduced radioactivity and bioluminescence signals. The results of monitoring therapeutic intervention in a doxorubicin dose series in vitro are presented in Figure 3. Higher doses of doxorubicin induced more SK-HEP1 and SK-HEP1-NL cell death (data not shown). After adriamycin treatment, the uptakes of radioiodide in SK-HEP1-NL cells were found to be proportional (r^2 = 0.9821) to the viable cell numbers (Fig. 3A). Similar to the result of radioiodide uptake, bioluminescence signals from SK-HEP1-NL cells were proportional to the cell numbers, as determined by luminescence assay and image (Fig. 3B).

In Vivo Image of Tumor Xenografted Mouse Model

For noninvasive quantitative monitoring of viable tumor burden, SK-HEP1-NL cells were inoculated. The injection of luciferin and the acquisition of bioluminescence image enabled the visualization of the viable tumor burden for SK-HEP1-NL, but the luminescence of SK-HEP1–induced tumors was not observed (Fig. 4A). A moderate correlation (r^2 = 0.7756) was observed between bioluminescence sig-

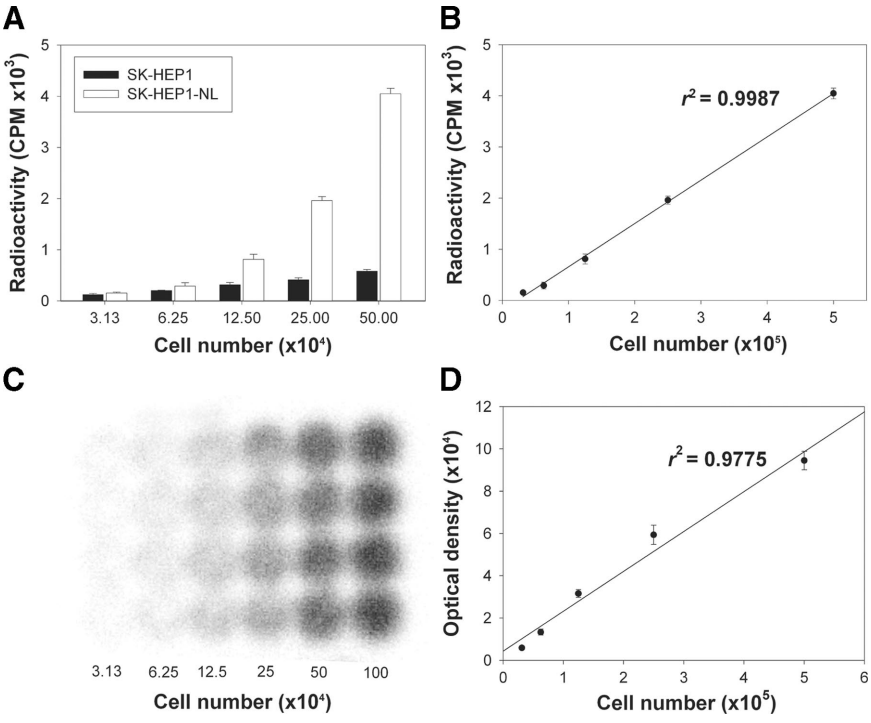

FIGURE 1. In vitro radioactivity assay according to cancer cell number. After inoculating a dilution series of SK-HEP1-NL cells (NIS expressing) and SK-HEP1 cells (control), radioiodine uptake assay and in vitro γ-camera image acquisition were performed. (A) Result of ^{125}I uptake shows similar accumulations regardless of SK-HEP1 cell number. In contrast, SK-HEP1-NL cells showed a significant increase of ^{125}I uptake according to cell number increase. (B) Linear regression analysis indicated high correlation between cell number and ^{125}I uptake. Correlation coefficient was r^2 = 0.9987. (C) ^{99m}Tc uptake in a dilution series of SK-HEP1-NL cells was visualized using a γ-camera. Higher numbers of cells (right line) showed more intense ^{99m}Tc uptake. (D) Linear regression analysis indicated high correlation between cell numbers and intensity of ROI in image (r^2 = 0.9775). OD of ROI was determined using image analysis program.

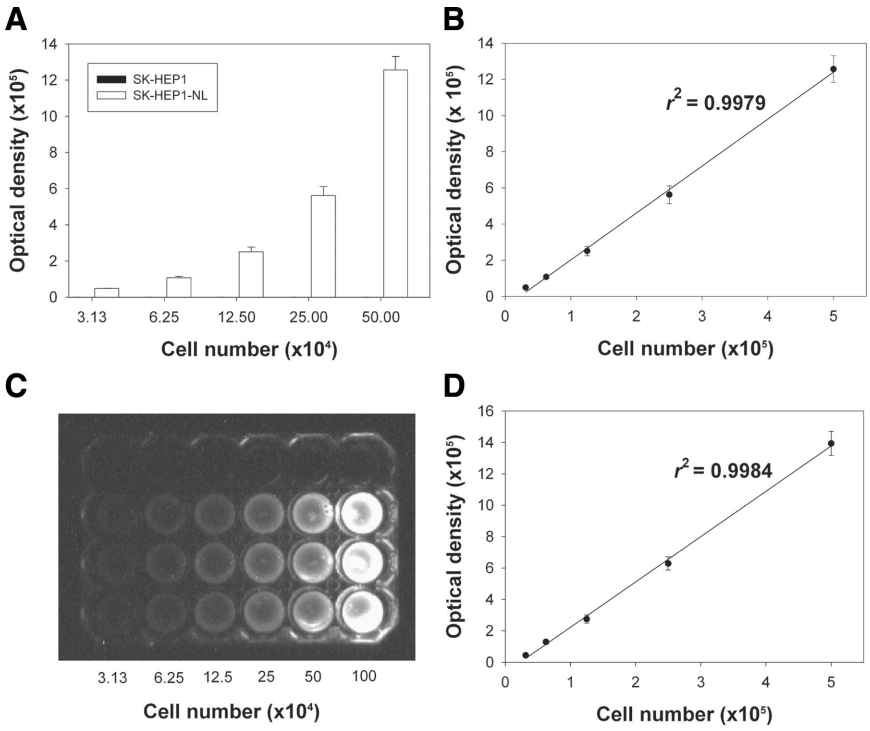

FIGURE 2. In vitro bioluminescence assay according to cancer cell number. After inoculating a dilution series of SK-HEP1-NL cells (NIS expressing) and SK-HEP1 cells (control), bioluminescence assay and in vitro bioluminescent image acquisition were performed. (A) Result of bioluminescence assay showed almost no luminescence change due to increased SK-HEP1 cell number. In contrast, SK-HEP1-NL showed significantly increased ^{125}I uptake as cell numbers increased. (B) Linear regression analysis indicated high correlation between cell number and bioluminescence ($r^2 = 0.9979$). (C) Bioluminescence of a dilution series of SK-HEP1-NL was visualized using a cooled CCD camera. Large number of cells (right line) showed intense luminescence. (D) Linear regression analysis indicated high correlation between cell number and intensity of ROI ($r^2 = 0.9984$). OD of ROI was measured using image analysis program.

nals and tumor weights (Fig. 4C). The injection of ^{99m}Tc-pertechnetate and the acquisition of a γ-camera image did enable the visualization of the SK-HEP1-NL viable tumor burden but did not allow this for SK-HEP1 tumors (Fig. 4B). A similar correlation was observed between the radioactivity, from the scintigraphic image, and the tumor weight (data not shown). Biodistribution data showed a higher correlation coefficient ($r^2 = 0.8661$) between radioactivity and tumor weight than that between the scintigraphic image intensity and tumor weight (Fig. 4D). A moderate correlation ($r^2 = 0.7782$) was observed between the OD from the bioluminescent image and the radioactivity from the tumor (Fig. 4E).

DISCUSSION

The rapid development of molecular imaging techniques enables the visualization of various events, such as gene delivery (*14*), endogenous gene expression (*15*), cell trafficking (*16*), signal transduction (*17*), apoptosis (*18*), tumor angiogenesis (*19*), and protein–protein interaction (*20*) noninvasively and repetitively in living organisms. In the fields of cancer research and anticancer drug development, these molecular imaging techniques have been used to visualize tumorigenesis, tumor cell growth (*21*), tumor metastasis (*5,22*), and the effect of therapy (*2,4*) using bioluminescent and fluorescent imaging techniques.

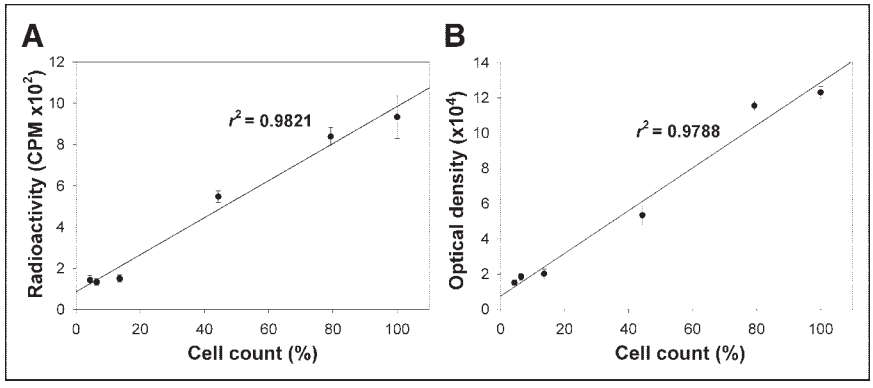

FIGURE 3. Correlation between cell counts and assay results after doxorubicin treatment. Various concentrations of doxorubicin (0, 0.5, 1, 2, 5, and 10 μg/mL) were administrated to 2×10^5 cells and incubated for 24 h. Viable cells were then counted by trypan blue exclusion. Viabilities of cells are presented as percentages. ^{125}I uptake or bioluminescence assay was performed. (A) Linear regression analysis was performed between ^{125}I uptake and viable cell count. Uptakes of radioiodide in SK-HEP1-NL were found to be proportional ($r^2 = 0.9821$) to viable cancer cell count. (B) Linear regression between ^{125}I uptake and viable cell count showed that bioluminescence signals were proportional ($r^2 = 0.9788$) to viable cancer cell count.

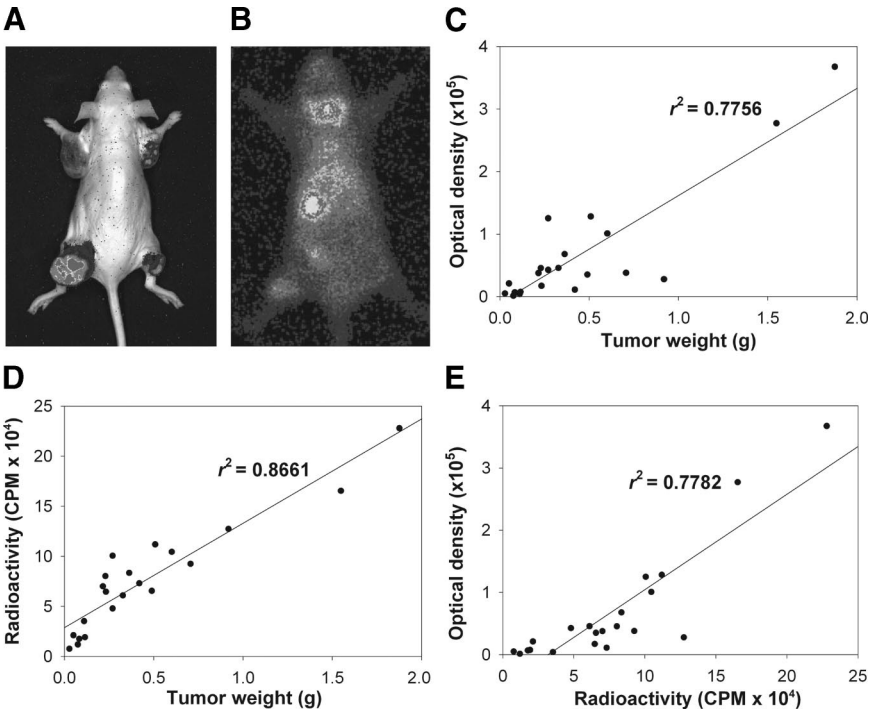

FIGURE 4. In vivo image of tumor xenografted mouse model. SK-HEP1 and SK-HEP1-NL cells were xenografted subcutaneously into left fore flank (SK-HEP1; 5×10^6 cells), right fore flank (SK-HEP1-NL; 5×10^6 cells), left hind flank (SK-HEP1-NL; 1×10^7 cells), and right hind flank (SK-HEP1-NL; 5×10^6 cells) of each mouse. After tumor growth, bioluminescent and γ-camera images were acquired, and biodistribution of radioactivity was investigated. (A) Injection of luciferin (126 mg/kg) and acquisition of bioluminescence image visualized viable tumor burden of SK-HEP1-NL cells, but not of SK-HEP1 cells. Left hind flank site was most highlighted, which was inoculated with largest number of cells. (B) Injection of ^{99m}Tc-pertechnetate and γ-camera imaging visualized viable tumor burden of SK-HEP1-NL cells, but not of SK-HEP1 cells. Using the same manner as that of the bioluminescent image, tumor on left hind flank site was most highlighted, which was inoculated with largest number of cells. (C) Correlation between bioluminescence signal and tumor weight (correlation coefficient, $r^2 = 0.7756$). (D) After acquisition of scintigraphic image, mice were sacrificed and biodistribution of radioactivity was examined. Correlation between tumor weight and radioactivity of each tumor is shown ($r^2 = 0.8661$). Correlation between radioactivity of biodistribution and tumor weight was higher than that between intensity of ROI from scintigraphic image and tumor weight. (E) Comparison of modality was estimated by plotting optical signal vs. radioactivity of tumors. Moderate correlation ($r^2 = 0.7782$) was observed between OD from bioluminescent image and radioactivity from tumors.

There are several modalities for molecular imaging in living organisms, such as fluorescent, bioluminescent, and nuclear imaging and MRI. Each modality has its own advantages and disadvantages. Fluorescent images dominate at the cellular level and, more recently, at the small animal level. Many cellular events can be visualized using fluorescent proteins and dyes under the microscope (*17,23–26*). Bioluminescence images are well established in small animal models using a cooled CCD camera. But these 2 optical approaches have limitations in large animal studies, especially in human applications, because of poor tissue penetration, whereas nuclear imaging and MRI are useful in large animals and in humans. Recent research, using these imaging modalities, has achieved many advances in small animal models. However, nuclear imaging, especially PET and MRI, are at a disadvantage because of their high cost and low research accessibility.

Because of such inherent weaknesses, no single modality can undertake this role from research to clinical application. In recent studies, a combination of each modality has been reported (*27–29*). Such multimodality approaches can overcome these limitations by using a dual- or triple-imaging reporter. These multimodality imaging reporters can be used in wide-range application from the cellular level to large animals (including humans). Recently, Gambhir's group reported a triple-fusion reporter that can be used at the cellular level (microscopic image, fluorescence-activated cell sorter) with a fluorescence probe, at the small living animal level with a bioluminescence probe, and at the large living animal level with a radionuclide probe (*29*). Making a fusion gene (*27,29*), linking by the IRES (*30,31*), dividing 2 reporter genes under a bidirectional promoter (*32*), placing both genes at separate locations in the same vector (*33*), and cotransferring both viral vectors at the same titer (*34*) can be used to connect a reporter gene. Because each approach has some disadvantages—such as alteration of the tertiary protein structure in a fusion protein or attenuation of the downstream gene in the case of the IRES approach—the choice of an optimal linkage method is necessarily dependent on each situation. We used the IRES method in this study because the location of the reporter genes differs (NIS is an intrinsic membrane protein and luc is a cytosolic protein). Recent studies reported that the efficiency of the IRES function depends on organs (*35–37*). Yanagiya et al. concluded that the tissue-specific activity of the IRES may be reflected in tissue tropism of a virus whose specific translation initiation is driven by the IRES (*36*). If one uses the current approach, the signal ratio of 2 genes that are linked by the IRES would be changed with different organs. After the bioluminescent imaging methods are established, immediate translation to clinical trials using well-established nuclear imaging in humans may be possible.

Recently, we found that the NIS gene has properties that make it suitable for use as an imaging reporter gene—the

most valuable advantage being its ease of application in humans (*38*). It requires only inexpensive and widely used radioiodines or ^{99m}Tc-pertechnetate and a γ-camera, which are available in most general hospitals worldwide. The size of the gene is small enough to deliver, and the NIS protein is not immunogenic because of its human origin.

The present study demonstrates the possibility of using the dual-reporter approach to measure the viable tumor cell burden and therapeutic effects noninvasively, repetitively, in vitro and in vivo. The reporter signals from both the nuclear approach and the optically based approach were highly correlated with cancer cell numbers in vitro. Next, we applied this method to evaluate the therapeutic effect of the anticancer drug doxorubicin; reduced viable cancer cell numbers were well correlated with the results obtained. In the animal experiments, nuclear and optical images detected xenografted tumors. The measured signals from the scintigraphic and bioluminescent image obtained reflected tumor weight, though they were not as proportional to tumor weight as were the results of in vitro results.

The advantage of evaluating the therapeutic effect of cancer cells using molecular imaging is that the method enables the measurement of viable cells only. Conventional evaluation methods of tumor mass rely on direct measurement of size, which is based on tumor anatomic mass. However, tumor mass consists of not only viable tumor cells but also necrotic and inflammatory regions, whereas molecular imaging counts only viable tumor cells. In this study, the correlation between tumor weights and signals was relatively poor in the tumor xenografted animal model compared with the in vitro monolayered cell culture. This difference might be because the signals from the animal experiment reflected only viable cells. We speculate that this molecular imaging is more accurate than conventional measurements of tumor size or weight for detecting viable cancer cells. In addition, early and more accurate changes in viable tumor cells can be detected by molecular imaging because the anatomic changes of tumors are observed during the later stages of therapy. The bioluminescent image in vivo showed a much lower correlation than that of the nuclear image. The optical signal can be influenced by several factors, including hemoglobin, water, and oxygen saturation (*39–42*). Hemoglobin and the red blood cell itself attenuate the light signal by absorption and scattering. Some investigators attempt to reduce this attenuation by using near-infrared light, a blood substitute, and so forth (*42*). In this study, tumor growth can result in angiogenesis, and the increase in vascularity can cause attenuation of the light signal by hemoglobin and the red blood cell. This can lead to a lack of correlation between the number of cells and the bioluminescence signal.

The disadvantage of the strategy used in this study is that it is limited to ex vivo or stable cell lines. The prerequisite of this strategy is the expression of the reporter in all viable cells during the time of interest. Because in vivo gene delivery to specific cells is limited, the manufacture of cells expressing the reporter gene must be undertaken before inoculation. Images acquired after gene delivery in vivo visualize not viable cells but, rather, the distribution of the delivered reporter gene.

CONCLUSION

The described modality using a dual-imaging reporter would be useful to evaluate the effects of various therapeutic approaches, such as chemotherapy, radiotherapy, gene therapy, and immunotherapy. Because of the advantages offered by a combination of optical and nuclear images, it is hoped that this technique will move quickly from in vitro and animal level study to clinical trials.

ACKNOWLEDGMENTS

This work was supported by grant 03-2002-013-0 from the Seoul National University Hospital research fund (2002), a research grant from the Cancer Research Institute, Seoul National University (2003), and the BK21 Project for Medicine, Dentistry, and Pharmacy (2003).

REFERENCES

1. Kim CG, Yang DJ, Kim EE, et al. Assessment of tumor cell proliferation using [^{18}F]fluorodeoxyadenosine and[^{18}F]fluoroethyluracil. *J Pharm Sci.* 1996;85:339–344.
2. Sweeney TJ, Mailander V, Tucker AA, et al. Visualizing the kinetics of tumor-cell clearance in living animals. *Proc Natl Acad Sci USA.* 1999;96:12044–12049.
3. Contag CH, Jenkins D, Contag PR, Negrin RS. Use of reporter genes for optical measurements of neoplastic disease in vivo. *Neoplasia.* 2000;2:41–52.
4. Chaudhuri TR, Mountz JM, Rogers BE, Partridge EE, Zinn KR. Light-based imaging of green fluorescent protein-positive ovarian cancer xenografts during therapy. *Gynecol Oncol.* 2001;82:581–589.
5. El Hilali N, Rubio N, Martinez-Villacampa M, Blanco J. Combined noninvasive imaging and luminometric quantification of luciferase-labeled human prostate tumors and metastases. *Lab Invest.* 2002;82:1563–1571.
6. Chung JK. Sodium iodide symporter: its role in nuclear medicine. *J Nucl Med.* 2002;43:1188–1200.
7. Spitzweg C, Dietz AB, O'Connor MK, et al. In vivo sodium iodide symporter gene therapy of prostate cancer. *Gene Ther.* 2001;8:1524–1531.
8. Min JJ, Chung JK, Lee YJ, et al. In vitro and in vivo characteristics of a human colon cancer cell line, SNU-C5N, expressing sodium-iodide symporter. *Nucl Med Biol.* 2002;29:537–545.
9. Cho JY, Shen DH, Yang W, et al. In vivo imaging and radioiodine therapy following sodium iodide symporter gene transfer in animal model of intracerebral gliomas. *Gene Ther.* 2002;9:1139–1145.
10. Petrich T, Helmeke HJ, Meyer GJ, Knapp WH, Potter E. Establishment of radioactive astatine and iodine uptake in cancer cell lines expressing the human sodium/iodide symporter. *Eur J Nucl Med Mol Imaging.* 2002;29:842–854.
11. Groot-Wassink T, Aboagye EO, Glaser M, Lemoine NR, Vassaux G. Adenovirus biodistribution and noninvasive imaging of gene expression in vivo by positron emission tomography using human sodium/iodide symporter as reporter gene. *Hum Gene Ther.* 2002;13:1723–1735.
12. Barton KN, Tyson D, Stricker H, et al. GENIS: gene expression of sodium iodide symporter for noninvasive imaging of gene therapy vectors and quantification of gene expression in vivo. *Mol Ther.* 2003;8:508–518.
13. Weiss SJ, Philp NJ, Grollman EF. Iodide transport in a continuous line of cultured cells from rat thyroid. *Endocrinology.* 1984;114:1090–1098.
14. Zinn KR, Douglas JT, Smyth CA, et al. Imaging and tissue biodistribution of ^{99m}Tc-labeled adenovirus knob (serotype 5). *Gene Ther.* 1998;5:798–808.
15. Doubrovin M, Ponomarev V, Beresten T, et al. Imaging transcriptional regulation of p53-dependent genes with positron emission tomography in vivo. *Proc Natl Acad Sci USA.* 2001;98:9300–9305.
16. Adonai N, Nguyen KN, Walsh J, et al. Ex vivo cell labeling with ^{64}Cu-pyruvaldehyde-bis(N4-methylthiosemicarbazone) for imaging cell trafficking in mice with positron-emission tomography. *Proc Natl Acad Sci USA.* 2002;99:3030–3035.

17. Ting AY, Kain KH, Klemke RL, Tsien RY. Genetically encoded fluorescent reporters of protein tyrosine kinase activities in living cells. *Proc Natl Acad Sci USA.* 2001;98:15003–15008.
18. Narula J, Acio ER, Narula N, et al. Annexin-V imaging for noninvasive detection of cardiac allograft rejection. *Nat Med.* 2001;7:1347–1352.
19. Bremer C, Tung CH, Weissleder R. In vivo molecular target assessment of matrix metalloproteinase inhibition. *Nat Med.* 2001;7:743–748.
20. Ray P, Pimenta H, Paulmurugan R, et al. Noninvasive quantitative imaging of protein-protein interactions in living subjects. *Proc Natl Acad Sci USA.* 2002;99: 3105–3110.
21. Edinger M, Sweeney TJ, Tucker AA, Olomu AB, Negrin RS, Contag CH. Noninvasive assessment of tumor cell proliferation in animal models. *Neoplasia.* 1999;1:303–310.
22. Yang M, Jiang P, Sun FX, et al. A fluorescent orthotopic bone metastasis model of human prostate cancer. *Cancer Res.* 1999;59:781–786.
23. Adams SR, Harootunian AT, Buechler YJ, Taylor SS, Tsien RY. Fluorescence ratio imaging of cyclic AMP in single cells. *Nature.* 1991;349:694–697.
24. Becker A, Hessenius C, Licha K, et al. Receptor-targeted optical imaging of tumors with near-infrared fluorescent ligands. *Nat Biotechnol.* 2001;19:327–331.
25. Chalfie M, Tu Y, Euskirchen G, Ward WW, Prasher DC. Green fluorescent protein as a marker for gene expression. *Science.* 1994;263:802–805.
26. Misteli T, Spector DL. Applications of the green fluorescent protein in cell biology and biotechnology. *Nat Biotechnol.* 1997;15:961–964.
27. Ray P, Wu AM, Gambhir SS. Optical bioluminescence and positron emission tomography imaging of a novel fusion reporter gene in tumor xenografts of living mice. *Cancer Res.* 2003;63:1160–1165.
28. Jacobs A, Dubrovin M, Hewett J, et al. Functional coexpression of HSV-1 thymidine kinase and green fluorescent protein: implications for noninvasive imaging of transgene expression. *Neoplasia.* 1999;1:154–161.
29. Ray P, De A, Min JJ, Tsien RY, Gambhir SS. Imaging tri-fusion multimodality reporter gene expression in living subjects. *Cancer Res.* 2004;64:1323–1330.
30. Tjuvajev JG, Joshi A, Callegari J, et al. A general approach to the non-invasive imaging of transgenes using cis-linked herpes simplex virus thymidine kinase. *Neoplasia.* 1999;1:315–320.
31. Yu Y, Annala AJ, Barrio JR, et al. Quantification of target gene expression by imaging reporter gene expression in living animals. *Nat Med.* 2000;6:933–937.
32. Baron U, Freundlieb S, Gossen M, Bujard H. Co-regulation of two gene activities by tetracycline via a bidirectional promoter. *Nucleic Acids Res.* 1995;23:3605–3606.
33. Bramson J, Hitt M, Gallichan WS, Rosenthal KL, Gauldie J, Graham FL. Construction of a double recombinant adenovirus vector expressing a heterodimeric cytokine: in vitro and in vivo production of biologically active interleukin-12. *Hum Gene Ther.* 1996;7:333–342.
34. Yaghoubi SS, Wu L, Liang Q, et al. Direct correlation between positron emission tomographic images of two reporter genes delivered by two distinct adenoviral vectors. *Gene Ther.* 2001;8:1072–1080.
35. Pilipenko EV, Viktorova EG, Guest ST, Agol VI, Roos RP. Cell-specific proteins regulate viral RNA translation and virus-induced disease. *EMBO J.* 2001;20: 6899–6908.
36. Yanagiya A, Ohka S, Hashida N, et al. Tissue-specific replicating capacity of a chimeric poliovirus that carries the internal ribosome entry site of hepatitis C virus in a new mouse model transgenic for the human poliovirus receptor. *J Virol.* 2003;77:10479–10487.
37. Forton DM, Karayiannis P, Mahmud N, Taylor-Robinson SD, Thomas HC. Identification of unique hepatitis C virus quasispecies in the central nervous system and comparative analysis of internal translational efficiency of brain, liver, and serum variants. *J Virol.* 2004;78:5170–5183.
38. Shin JH, Chung JK, Kang JH, et al. Feasibility of sodium/iodide symporter gene as a new imaging reporter gene: comparison with HSV1-tk. *Eur J Nucl Med Mol Imaging.* 2004;31:425–432.
39. Roggan A, Friebel M, Dorschel K, Hahn A, Müller G. Optical properties of circulating human blood in the wavelength range 400–2500 nm. *J Biomed Opt.* 1999;4:36–46.
40. Steinke JM, Shepherd AP. Role of light scattering in whole blood oximetry. *IEEE Trans Biomed Eng.* 1986;33:294–301.
41. Kramer K, Elam JO, Saxton GA, Elam WN Jr. Influence of oxygen saturation, erythrocyte concentration and optical depth upon the red and near-infrared light transmittance of whole blood. *Am J Physiol.* 1951;165:229–246.
42. Villard JW, Feldman MD, Kim J, Milner TE, Freeman GL. Use of a blood substitute to determine instantaneous murine right ventricular thickening with optical coherence tomography. *Circulation.* 2002;105:1843–1849.